Electronic Supporting Information for

Computational Design of an Iridium based Catalyst for Releasing H_2 from Hydrogenated BN Nanotube

Lisa Roy and Ankan Paul**

Raman Centre for Atomic Molecular and Optical Sciences, Indian Association for the Cultivation of Science, Kolkata - 700032, India.
*Corresponding author: E-mail: rclr@iacs.res.in, rcap@iacs.res.in

Contents

S17) Gaussian 09 full citation

S18) References

S1) General information on quantum chemical methods employed

a) Computational details

All the geometries were optimized in vacuum with hybrid exchange-correlation B3LYP functional in conjunction with Pople's basis set as implemented in Gaussian09 quantum chemical package. B3LYP has been the chosen functional for all the optimizations as it has been reported to correctly describe the geometry of species studied in the catalytic reactions of analogous Iridium pincer complexes.[1-3] Furthermore the choice of B3LYP was also based on the success of the method in theoretical studies of the chemistry of single-walled carbon and boron nitride nanotubes by various groups.[4-5] Harmonic frequencies were computed to characterize the structures as minimum (all real frequencies) and transition state (one imaginary mode) and also to extract thermo-chemical information. In addition, intrinsic reaction coordinate (IRC) analysis was carried out to confirm the connection between reactant, product and transition state.[6] HBNNTs has been optimized with B1 basis set combination where four adjacent benzenoid rings in the reaction locale have been given 6-31++G(d,p) basis set while the remaining part of the system have been optimized with minimal basis STO-3G; catalysts has been optimized with 6-31++G(d,p) on all the non-metals barring the *iso*propyl groups which are given 6-31G(d) basis along with LANL2DZ basis and LANL2 ECP on the Ir centre. Following this, single point solvent phase computations on the B3LYP[7a] optimized geometries were carried out at M06L[7b], M06L-GD3,[7c] B3LYP-GD3[7c] and ωB97x-D[7d] functionals employing B3 basis set combination for 1-HBNNT and B3' basis set combination for 2-HBNNT. The CPCM model[8] which gives fairly reliable result for solid-solvent interaction has been chosen as the solvent model with the Universal Force Field (UFF) radii. The dielectric constant in the CPCM calculations was set to 7.4257 to simulate tetrahydrofuran, which was the solvent medium for the experimental and theoretical dehydrogenation of AB by the Brookhart catalyst (**Ir_{tBu}**).[9,1] To check the sensitivity of the predicted barriers on basis sets and functional, we have re-optimized some crucial intermediates and transition states using B3LYP, M06L and M06L-GD3 with B2 basis set for 1-HBNNT and B2' for 2-HBNNT (see Table 1). It was interesting to note that apart from the similarity in the molecular geometries between those optimized at B3LYP/B1 and B3LYP/B2 level of theory, we also found that computing a single SCF calculation at M06L/B3 level of theory on these 2 different geometries yielded similar energy barriers in both gas and solvent phase. Furthermore, the barriers were checked with optimizations at M06L/B2 and M06L-GD3/B2 level of theory, followed by solvent phase single point calculation with different functionals. The deviations were within ~ 1-1.5 kcal mol^{-1}. For 2-HBNNT we re-optimized at B3LYP/B2' and did single point solvent phase calculations at different levels of theory and found comparable energetics with the previous results. See section S8 for all the predicted barriers. The Gibbs free energy barriers and total energy barriers being comparable at two different levels of theory clearly suggests the reliability of the method chosen by us and validates the approximation of using minimal basis set for optimization of larger part of the nanotube.

Gas phase enthalpies and Gibbs free energies are computed by adding enthalpic corrections and Gibbs free energy corrections respectively to the total energies at 298.15 K and 1 atm. However for solvent phase calculations, Gibbs free energies were modified. This is due to the fact that in the ideal gas model the damping of translational and rotational degrees of freedom in solvent phase gets ignored and the entropy is overestimated. To compensate such a situation many techniques are prevalent in computational chemistry literatures. Martin and co-workers proposes to artificially raise the pressure of a system from 1 to 1354 atm which corresponds to a free energy correction of 4.3 kcal mol^{-1}.[10a] Wertz[10b] and Spickermann[10c] are of the opinion that entropy of a solute should be estimated to be 0.46S(g) or 0.67S(g) where S(g) is the entropy of the solute in gas phase. Furthermore, experiments by Yu and Houk[10d] have demonstrated that the ideal gas model could overestimate the entropic contribution for bimolecular reaction by 50−70%. Hence on the basis of previous reports,[11] corrected Gibbs free energies were computed using solvent phase entropies, which in turn were derived by scaling gas phase entropies

by an empirical factor of 0.5. It must be noted that application of the correction scheme does not overrule our proposed reaction mechanism. For validation we have provided zero-point corrected total energy values in the tables in S8. ΔG indicates relative free energy and ΔE_{ZP} is the zero-point corrected relative electronic energy in gas or solvent phase as stated.

*Table 1. B*asis set combination

Basis set combination	**Basis set used for BN nanotube**		**Basis set used for catalyst**	
	Basis given on the reactive zone	Basis given on the rest of the nanotube	Basis function and ECP given on metal	Basis given on the pincer ligands and *iso*propyl groups
B1	6-31++G(d,p)	STO-3G	LANL2DZ, LANL2	6-31++G(d,p), 6-31G(d)
B2	6-31++G(d,p)	6-31G(d)	LANL2DZ, LANL2	6-31++G(d,p), 6-31G(d)
B2'	6-31++G(d,p) on high layer, 6-31G(d) on medium layer	STO-3G	LANL2DZ, LANL2	6-31++G(d,p), 6-31G(d)
B3	6-31++G(d,p)	6-31++G(d,p)	LANL2DZ, LANL2	6-31++G(d,p)
B3'	6-31++G(d,p)	6-31G(d)	LANL2DZ, LANL2	6-31++G(d,p), 6-31G(d)

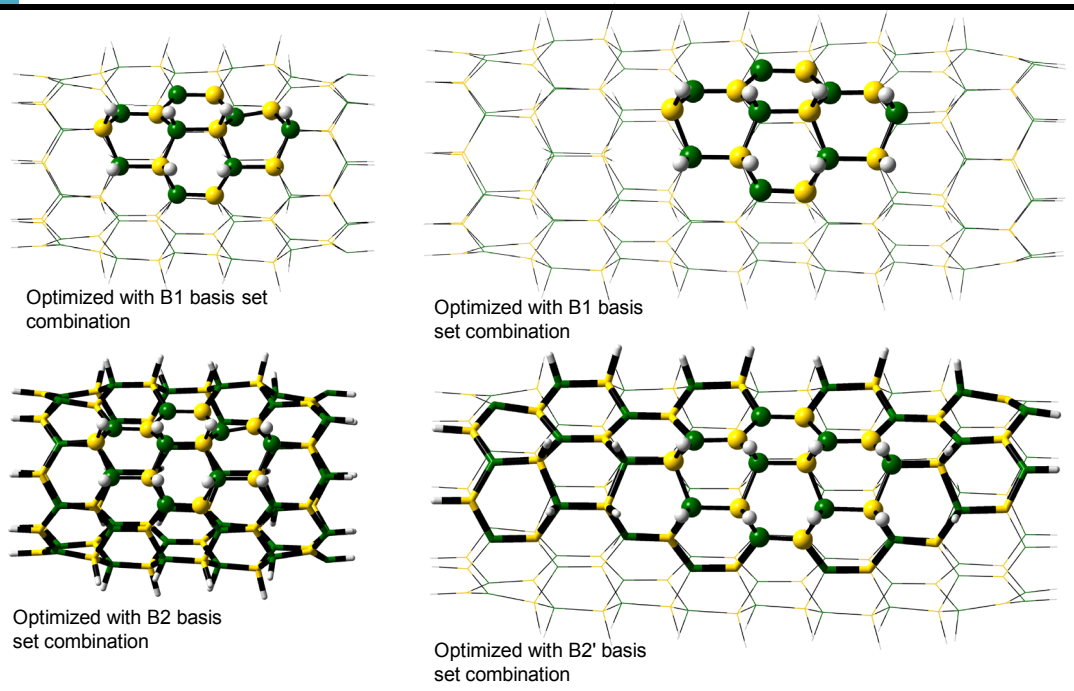

Figure 1. The picture above is a representation of the basis set combination used during optimization. Atoms represented by balls and tubes are treated as the “reactive zone” while those shown by wireframe are said to be the “rest of the nanotube”.

b) Molecular Models used

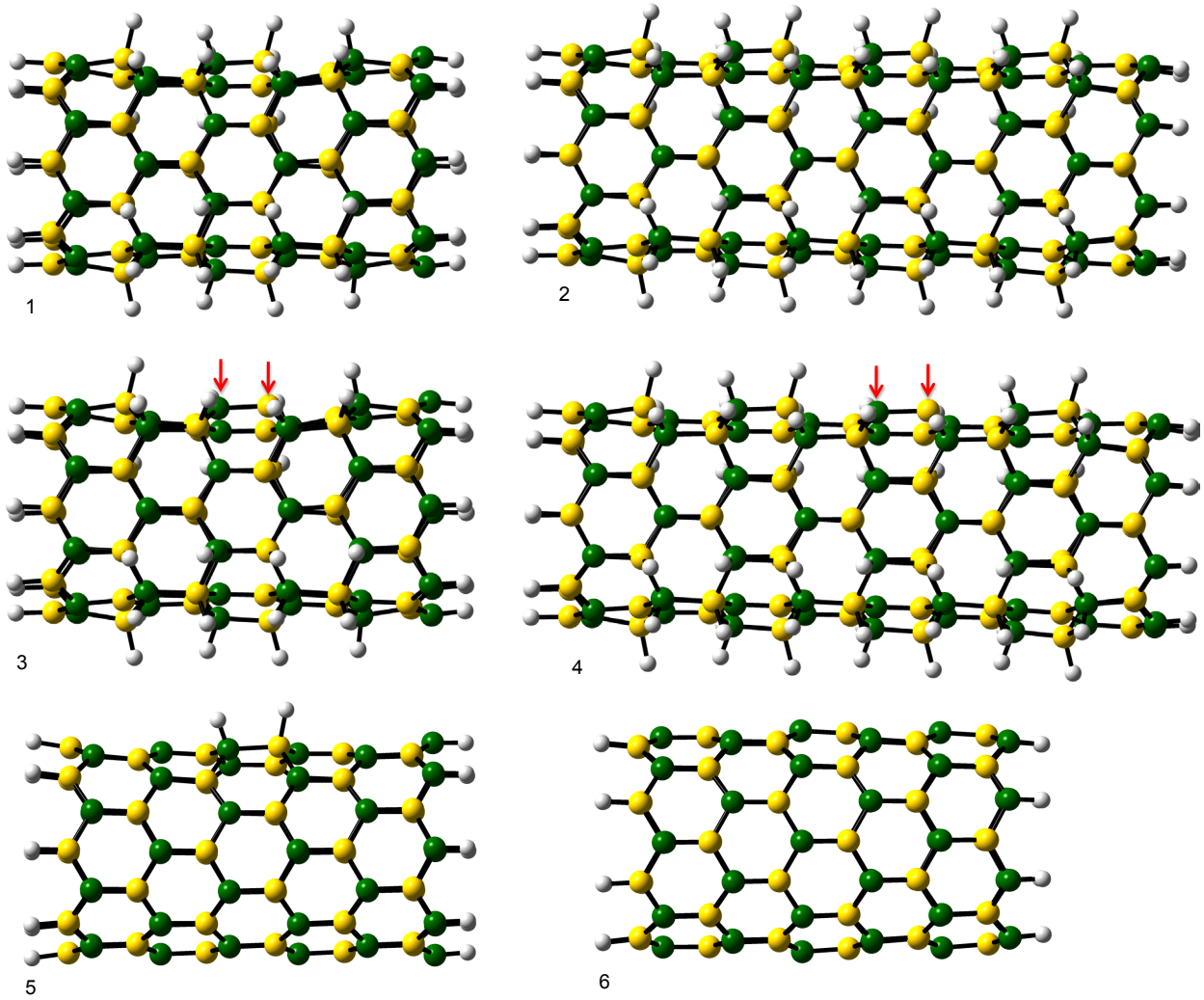

Figure 2. Chemisorbed hydrogenated and non-hydrogenated BN nanotube models used are 1) 1-HBNNT, 2) 2-HBNNT, 3) (1-HBNNT)-H_2, 4) (2-HBNNT)-H_2, 5) 1-SHBNNT, 6) BNNT.

S2) Dissociative pathway

In the dissociative pathway, free dihydrogen loss from **1** is followed by non-covalent interaction between the co-ordinatively unsaturated Ir centre of **1a** and one of the B-H hydrides chosen at the middle of a nanotube. We could locate a transition state (**TS1-1a**) for dissociation of H_2 from **1** which was unobserved in the previous computational studies of dehydrogenation of alkanes and ammonia borane with traditional pincer complexes.[1,2] Our computations show that the formation of **1a** (the bare catalyst) is endoergic with $\Delta G(s)_{SPC}$ = 15.6 kcal mol^{-1} at M06L(CPCM). Furthermore the enthalpy cost (which corresponds to thermal electronic energy with corrected zero-point vibrational energies) associated with dissociation of H_2 from **1** in the solution phase is found to be 18.4 kcal mol^{-1}, which is slightly higher than the predicted value of 15.7 kcal mol^{-1} at B3LYP(CPCM) by Paul and Musgrave.[1] However, the free energy activation barrier of **TS1-1a** in solvent phase is predicted to be 16.7 kcal mol^{-1}, implying the backward reaction to be significantly more favorable. Moreover the overall activation barrier to hydrogen loss from **1** in connection to **3** is calculated to be ~ 35 kcal mol^{-1} in both THF and gas-phase suggesting that the energy barrier is prohibitively high for the reaction to occur under moderate conditions. This is

in agreement with the previous findings by Goldman and co-workers for self-dehydrogenation of analogous iridium complexes.[2] Ligation of the bare catalyst, **1a**, to one of the hydrides on the reactive BN framework of 1-HBNNT displays σ B-H donation to vacant metallic d orbital. This is evident from the Frontier Molecular Orbitals of **1a** which displays significant contribution to both HOMO and LUMO from the d orbitals centred on the metal (discussed in S10). The formation of this intermediate (**2**) is a thermoneutral process with respect to **1** and 1-HBNNT and about 19.4 kcal mol^{-1} above intermediate **3** (see S5). A transition state (**TS2-1**) for the concerted transfer of proton and hydride from the hydrogenated nanotube identified for 1-HBNNT (see scheme in S4) with an imaginary frequency of *i*1192 cm^{-1} is predicted to overcome $\Delta G^{\ddagger}(s)$ = 13.5 and 32.6 kcal mol^{-1} from separated reactants and **3** respectively. The free energy of activation for an analogous transition state (**TS2'-1**) for 2-HBNNT is also similar (14.0 kcal mol^{-1}). This is in congruence to a similar 5-membered transition state in AB, $\mathbf{TS2_{AB}\text{-}1}$, with simultaneous dehydrogenation by **1a** overcoming a Gibbs free energy of activation of 15.1 kcal mol^{-1}. The corresponding gas phase free energy of activation for **TS2-1** (16.4 kcal mol^{-1}) and **TS2'-1** (16.9 kcal mol^{-1}) are also comparable. This transition state is followed by regeneration of **1** and separation of it from a hydrogenated BNNT, (1-HBNNT)-H_2.

S3) Dehydrogenation with a computationally designed catalyst, $\mathbf{Ir_{iPr}}$

DFT calculations showed MeO-PCP and POCOP ligands have similar kinetic and thermodynamic effects, relative to the parent PCP ligand, regardless of more electron richness of MeO-PCP complexes.[2] Hence to draw an analogy between the two structurally different but electronically similar catalysts, we tried to investigate the removal of chemisorbed hydrogens on BNNTs with analogous Ir catalysts, $\mathbf{Ir_{iPr}}$, (POCOP*i*Pr)Ir$(H)_2$, which is structurally equivalent to $\mathbf{Ir_{tBu}}$ barring the replacement of $t\mathrm{Bu_2P}$ groups with $i\mathrm{Pr_2P}$ in the POCOP ligand. Examination of the proton and hydride transfer to $\mathbf{Ir_{tBu}}$ from 1-HBNNT is observed at $\Delta G^{\ddagger}(s)$ = 19.7 kcal mol^{-1} while the subsequent dihydrogen release from the catalyst is predicted to occur at 18.0 kcal mol^{-1}. The free energy barriers are consistent with the catalytic dehydrogenation of 1-HBNNT by **1**. These comparable results of catalytic dehydrogenation of 1-HBNNT with both the Ir complexes opine that chemisorbed hydrogen atoms on hydrogenated BN nanotubes are vulnerable to dehydrogenation following a concerted removal from the nanotube surface and that too at moderate conditions; room to slightly elevated temperatures.

We have also devised strategy to synthesize $\mathbf{Ir_{iPr}}$. For the synthesis of bis(phophinite) PCP ligands, Brookhart et. al. has undertaken the approach[12] earlier followed by Jensen and his group for the synthesis of related Pd complexes.[13] There they had prepared 1,3-bis(diisopropylphosphinito)benzene starting from resorcinol in presence of chlorodiisopropylphosphine in THF medium. So we presume that for an analogous Ir catalyst, similar resorcinol and *iso*propyl substituted phosphine may be taken as the starting materials. However, the reaction conditions or the solvent medium may be different. The following schematic representation shows our proposed synthetic strategy to design $\mathbf{Ir_{iPr}}$.

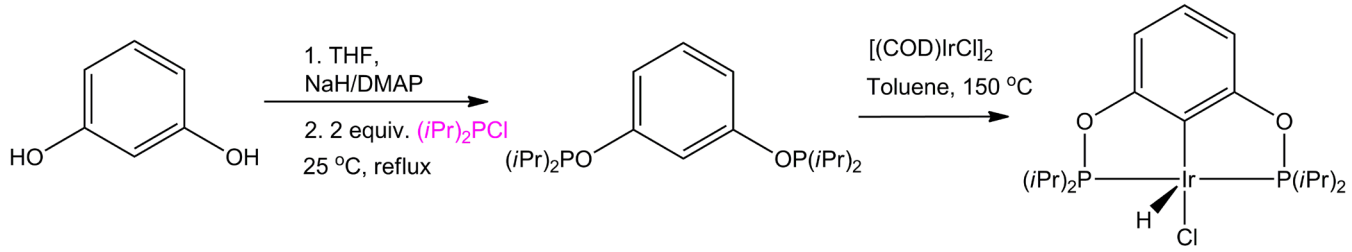

Scheme 1. Scheme for synthesizing *iso*propyl substituted POCOP pincer ligated Iridium complex

S4) Proposed mechanism of Ir (species 1) catalyzed dehydrogenation of chemisorbed hydrogenated BN nanotube (1-HBNNT) through dissociative and associative pathway

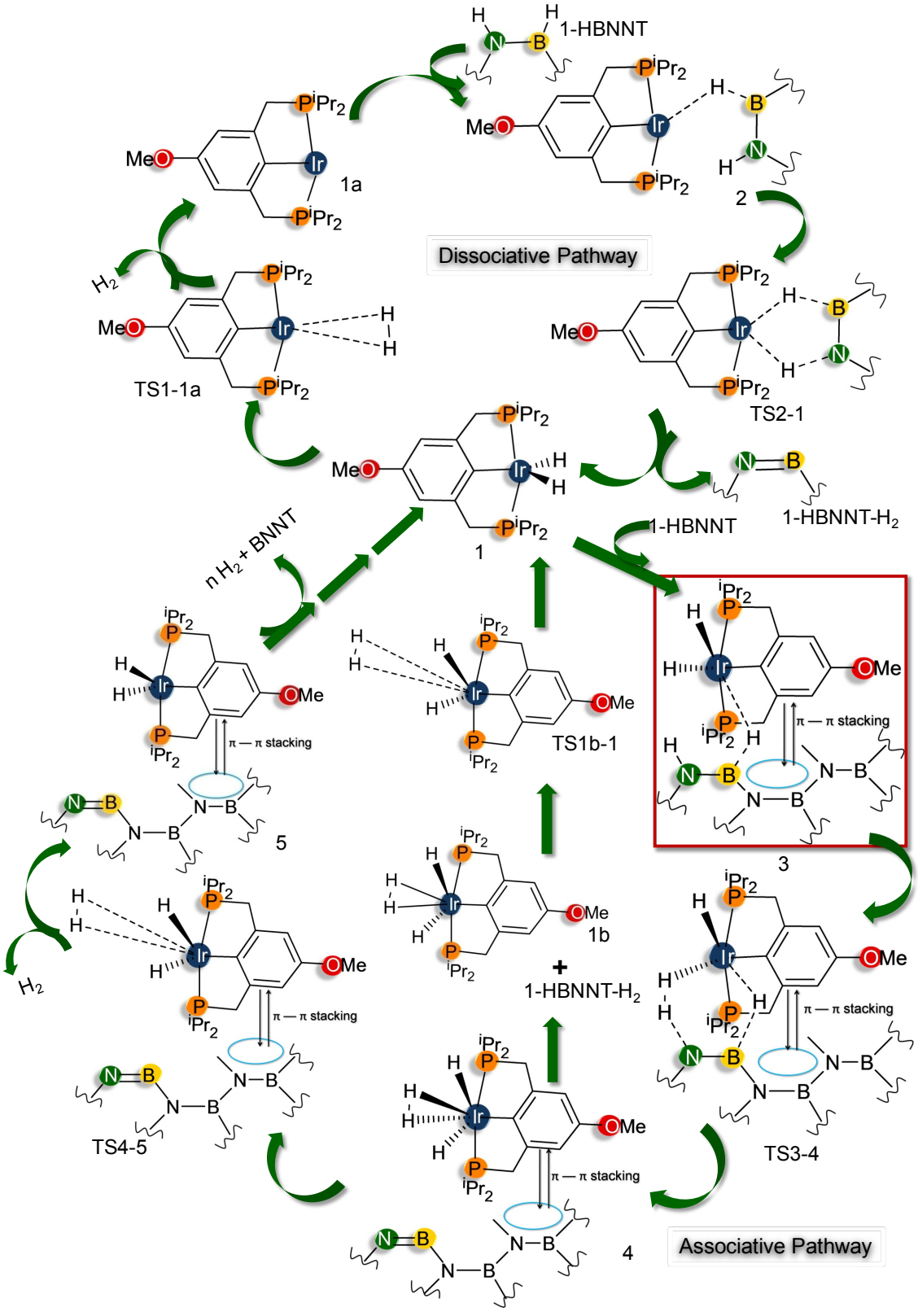

S5) Gibbs free energy profile for the dehydrogenation of 1-HBNNT with 1 in solvent phase at M06L/B3/B3LYP/B1

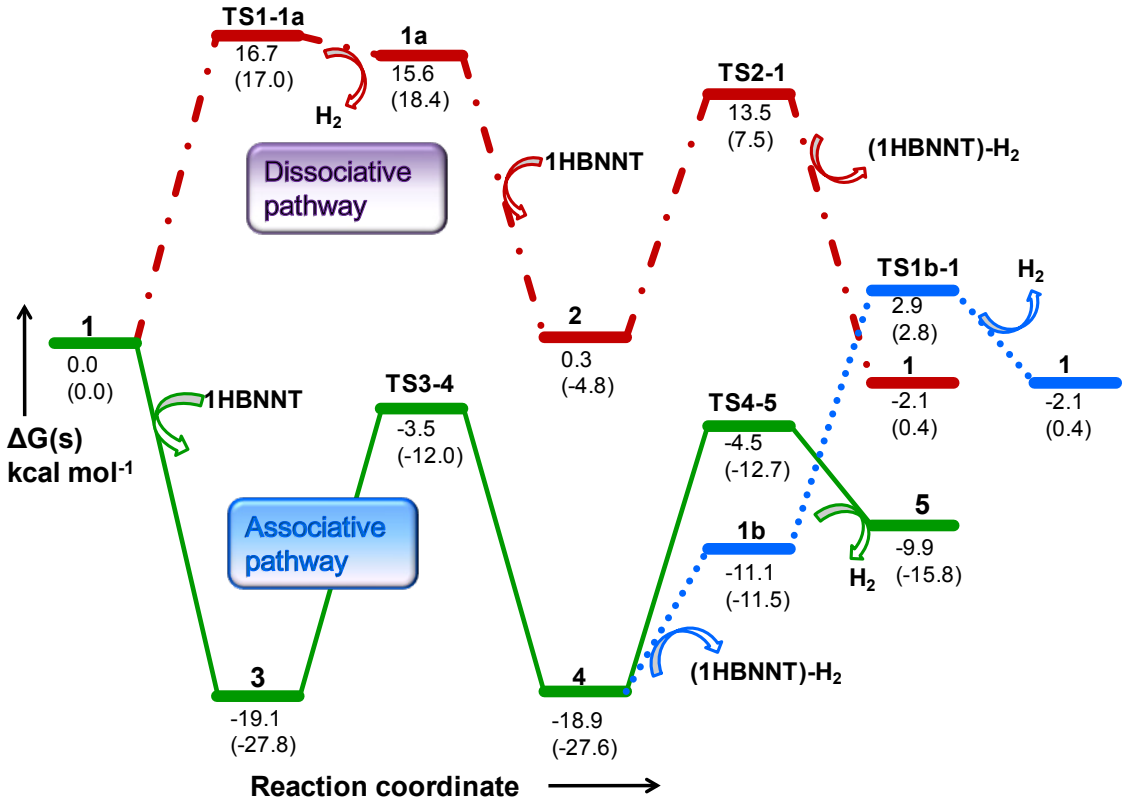

S6) Removal of a 2nd and the last H_2 molecule from 1-HBNNT with catalyst 1

Hydrogenation of a pristine non-hydrogenated BNNT is an overall endoergic process. The first H_2 attachment to a B=N bond at the middle of a non-hydrogenated 1 nm (8,0) zigzag BNNT with hydrogenated terminals takes place at a Gibbs free energy change of 24.7 kcal mol^{-1} with regard to the initial free reactants at M06L//B3LYP level of theory. Subsequent hydrogenation of BNNT takes place at similar free energy changes. The penultimate hydrogenation occurs at $\Delta G(s)$ = 18.8 kcal mol^{-1} and the ultimate H_2 addition is predicted to occur at 17.8 kcal mol^{-1}. So we hypothesized that the dehydrogenation probability would follow an inverse kinetics, with the first H_2 removal being the highest in barrier and the last one occurring at the lowest barrier.

In the main text we have shown how the catalyst (**1**) is regenerated via removal of H_2 by self-dehydrogenation (**TS4-5**), while weakly adsorbed on the hydrogenated BN nanotube surface. In the following intermediate, **5**, the dihydride Ir complex is regenerated and dihydrogen molecule is lost. To ensure the sustainability of the catalytic process, we investigated another dehydrogenation of the hydrogenated BNNT, (1-HBNNT)-H_2, aided by **1.** Since the removal of H_2 as gaseous dihydrogen molecule disrupts the equilibrium, we consider a new profile for the later part of the reaction. Initial favorable interaction between the B-H moiety of (1-HBNNT)-H_2 and **1** leads to the formation of **6** which is an exothermic process, similar to the previous instance. Thereby a concerted removal of hydride and proton from the BN nanotube surface is also observed which occurs through **TS6-7** at a lower free energy barrier (10.5 kcal mol^{-1}) (see *Figure 6*) as compared to its predecessor, **TS3-4**. $\Delta G^{\ddagger}(s)$ for an analogous second H_2 removal by catalyst **1** from 2-HBNNT is predicted to take place at 12 kcal mol-1 at M06L/B3'//B3LYP/B1 level of theory. The tetrahydride Ir complex then undergoes self-dehydrogenation while adsorbed on the nanotube surface for 1-HBNNT via **TS7-8** which ultimately give rise to another intermediate. This intermediate (**8**) is characterized by the regeneration of the dihydride Ir complex while adhered on the surface of the hydrogenated nanotube (1-HBNNT)-$2H_2$. The escape of the dihydrogen molecule via **TS7-8** is predicted to take place at a Gibbs free energy of activation of 15.4 kcal mol^{-1} which is comparable to the

predicted barriers for the first hydrogen removal by catalyst **1**. This suggests that akin to the previous desorption of H_2 from the HBNNT surface by complex **1**, subsequent dehydrogenation would also be feasible.

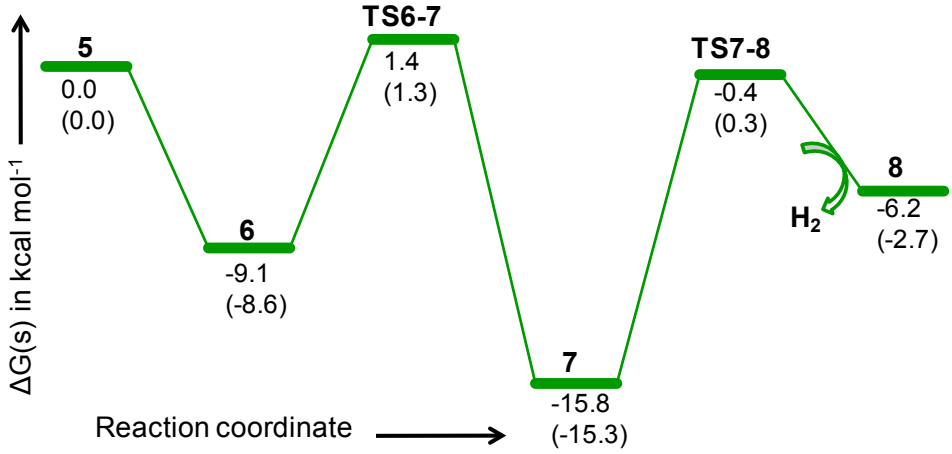

Figure 6. Solvent phase Gibbs free energy profile diagram for the 2nd H_2 dehydrogenation from 1-HBNNT with catalyst **1** starting from intermediate **5** at M06L/B3//B3LYP/B1. Solvent-phase zero-point corrected total energy values are given in parenthesis.

S7) Removal of the last H_2 molecule from a HBNNT with catalyst 1

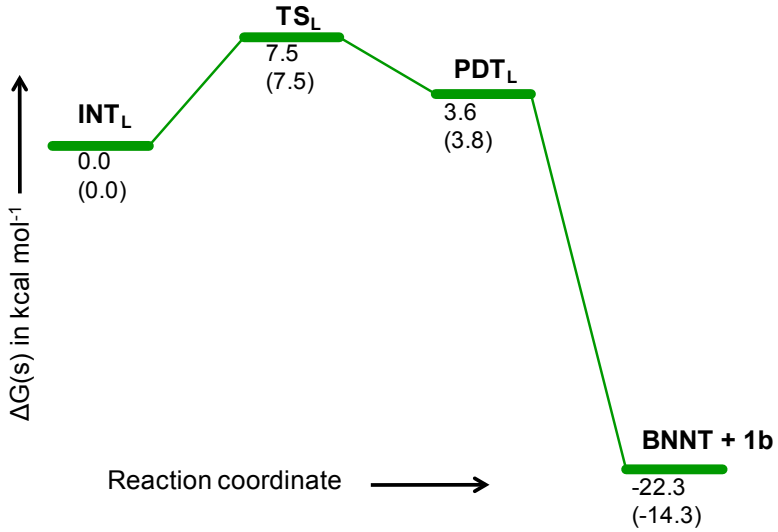

Figure 7. Solvent phase Gibbs free energy profile diagram for the last H_2 dehydrogenation starting from a 1-SHBNNT. Solvent-phase zero-point corrected total energy values are given in parenthesis.

One may be apprehensive of the dehydrogenation process to continue at low weight percentage content of hydrogen on the BN nanotube surface. Contrary to the presumption that decrease in quantity of chemisorbed hydrogen atoms from a HBNNT would decrease the possibility of dehydrogenation, we find that dehydrogenation from a mono-hydrogenated BN unit at the middle of a 1 nm long BNNT with hydrogenated terminals (1-SHBNNT) with **1** occurs with equal ease as its predecessors, 1-HBNNT and (1-HBNNT)-H_2. The desorption of hydrogen from 1-SHBNNT occurs at a further lower barrier, i.e $\Delta G^{\ddagger}(s)$ =7.5 kcal mol^{-1} via $\mathbf{TS_L}$ (see Figure 7). Thereby we obtain an intermediate $\mathbf{PDT_L}$ where $Ir(H)_4$ is weakly bounded to the pristine nanotube through non-covalent interaction. This intermediate lies at ~ 4 kcal mol^{-1} above $\mathbf{INT_L}$ while the separation of the pristine nanotube (BNNT) from **1b** is a highly exergonic process, being -22.3 kcal mol^{-1} compared to $\mathbf{INT_L}$. It is presumed that absence of the favorable Ir-H-B covalent interaction in $\mathbf{PDT_L}$ along with lack of C-H/π and π-π interaction

triggers removal of the tetrahydride Iridium complex from BNNT and explains the lowering of energy. This observation further supports that all the chemisorbed hydrogen atoms can be desorbed from the nanotube surface by **1** leaving behind non-hydrogenated BN nanotube which could be easily separated from the catalyst and recycled to attain sustainability. Furthermore since separation of the nanotube and the tetrahydride complex is favorable than there binding, the rate determining barrier in this case would be governed by the self desorption process, i.e. $\Delta G^{\ddagger}(s)$ of **TS1b-1** with respect to **1b** = 14 kcal mol^{-1}. So we see that contrary to usual belief, subsequent dehydrogenation of the hydrogenated BN nanotube would be possible with catalyst **1**.

S8) Tables for gas phase and solvent phase total energy barriers and Gibbs free energy barriers for the associative pathway

Relative free energies, ΔG(s) has been computed empirically with S(s)=0.5S(g) where S(g) is the gas phase entropy and S(s) is the solvent phase entropy. The general trend for barriers is as follows: M06L-GD3 ~ M06L < B3LYP-D3 < ωB97x-D.

*a) Dehydrogenation of 1-HBNNT with **1***

1) optimized at B3LYP/B1 and then single point calculations with the respective functionals with B3 basis set

	$\Delta E_{ZP}(g)_{M06L}$	$\Delta G(g)_{M06L}$	$\Delta E_{ZP}(s)_{M06L}$	$\Delta G(s)_{M06L}$	$\Delta G(s)_{M06L\text{-}GD3}$	$\Delta G(s)_{B3LYP\text{-}GD3}$	$\Delta G(s)_{\omega B97x\text{-}D}$
TS3-4	17.2	16.9	15.8	15.6	15.0	14.4	17.0
TS4-5	17.9	15.7	15.1	14.6	15.4	19.4	23.4
TS1b-1 (w.r.t 3)	43.7	25.3	30.6	22.0	30.7	33.2	42.7

2) optimized at B3LYP/B2 and then single point calculations with the respective functionals with B3 basis set

	$\Delta G(s)_{M06L}$	$\Delta G(s)_{M06L\text{-}GD3}$	$\Delta G(s)_{B3LYP\text{-}GD3}$	$\Delta G(s)_{\omega B97x\text{-}D}$
TS3-4	15.6	15.4	15.2	18.1
TS4-5	13.1	13.3	14.8	19.8
TS1b-1 (w.r.t 3)	25.5	33.2	34.6	42.7

3) optimized at M06L/B2 and then single point calculations with the respective functionals with B3 basis set

	$\Delta G(s)_{M06L}$	$\Delta G(s)_{M06L\text{-}GD3}$	$\Delta G(s)_{B3LYP\text{-}GD3}$	$\Delta G(s)_{\omega B97x\text{-}D}$
TS3-4	16.1	15.8	14.9	17.8
TS4-5	16.9	16.9	17.6	21.5
TS1b-1 (w.r.t 3)	31.2	39.2	39.0	49.1

4) optimized at M06L-GD3/B2 and then single point calculations with the respective functionals with B3 basis set

	$\Delta G(s)_{M06L}$	$\Delta G(s)_{M06L\text{-}GD3}$	$\Delta G(s)_{B3LYP\text{-}GD3}$	$\Delta G(s)_{\omega B97x\text{-}D}$
TS3-4	16.0	15.7	14.8	17.7
TS4-5	16.4	16.4	17.0	21.1
TS1b-1 (w.r.t 3)	30.8	38.8	37.9	48.1

*b) Dehydrogenation of 2-HBNNT by **1***

1) Optimized at B3LYP/B1 and then single point calculations with the respective functionals with B3' basis set

	$\Delta E_{ZP}(g)_{M06L}$	$\Delta G(g)_{M06L}$	$\Delta E_{ZP}(s)_{M06L}$	$\Delta G(s)_{M06L}$	$\Delta G(s)_{M06L\text{-}GD3}$	$\Delta G(s)_{B3LYP\text{-}GD3}$	$\Delta G(s)_{\omega B97x\text{-}D}$
TS3'-4'	14.6	14.3	15.9	15.7	14.7	14.3	17.4
TS1b-1 (w.r.t 4')	34.1	15.4	27.3	18.6	26.6	31.1	36.9

2) Optimized at B3LYP/B2 and then single point calculations with the respective functionals with B3' basis set

	$\Delta G(s)_{M06L}$	$\Delta G(s)_{M06L\text{-}GD3}$	$\Delta G(s)_{B3LYP\text{-}GD3}$	$\Delta G(s)_{\omega B97x\text{-}D}$
TS3'-4'	15.0	14.7	14.6	17.2
TS1b-1 (w.r.t 4')	21.3	29.3	34.3	40.8

*c) Dehydrogenation of AB by **1***

	$\Delta E_{ZP}(g)_{M06L}$	$\Delta G(g)_{M06L}$	$\Delta E_{ZP}(s)_{M06L}$	$\Delta G(s)_{M06L}$	$\Delta G(s)_{B3LYP\text{-}GD3}$	$\Delta G(s)_{\omega B97x\text{-}D}$
$TS3_{AB}$-1b	10.0	10.7	13.4	13.6	12.7	14.8
TS1b-1	20.4	14.5	20.2	14.7	14.4	17.3

*d) Dehydrogenation of 1-HBNNT by **Ir_{iPr}***

	$\Delta E_{ZP}(g)_{M06L}$	$\Delta G(g)_{M06L}$	$\Delta E_{ZP}(s)_{M06L}$	$\Delta G(s)_{M06L}$	$\Delta G(s)_{B3LYP\text{-}GD3}$	$\Delta G(s)_{\omega B97x\text{-}D}$
TS3"-4"	19.9	20.1	19.6	19.7	18.0	20.8
TS4"-5"	19.3	17.0	17.8	18.0	19.9	23.6
$TSIr_{iPr}b\text{-}Ir_{iPr}$ (w.r.t 4")	46.7	30.2	37.3	29.1	38.1	46.9

S9) Optimized geometries of important intermediates and transition states

In all the geometries bond distances are given in units of Å. For color coding see main text.

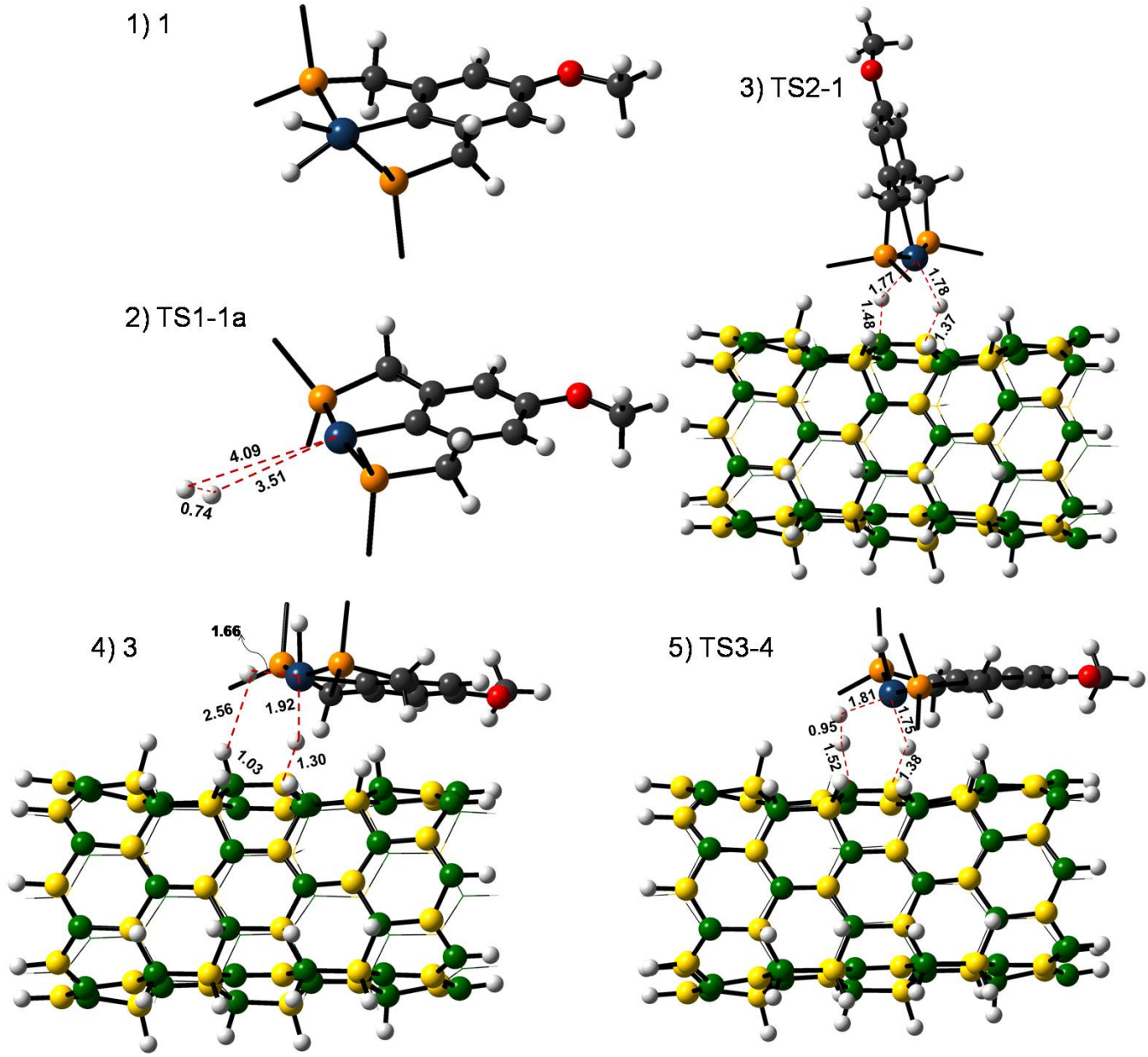

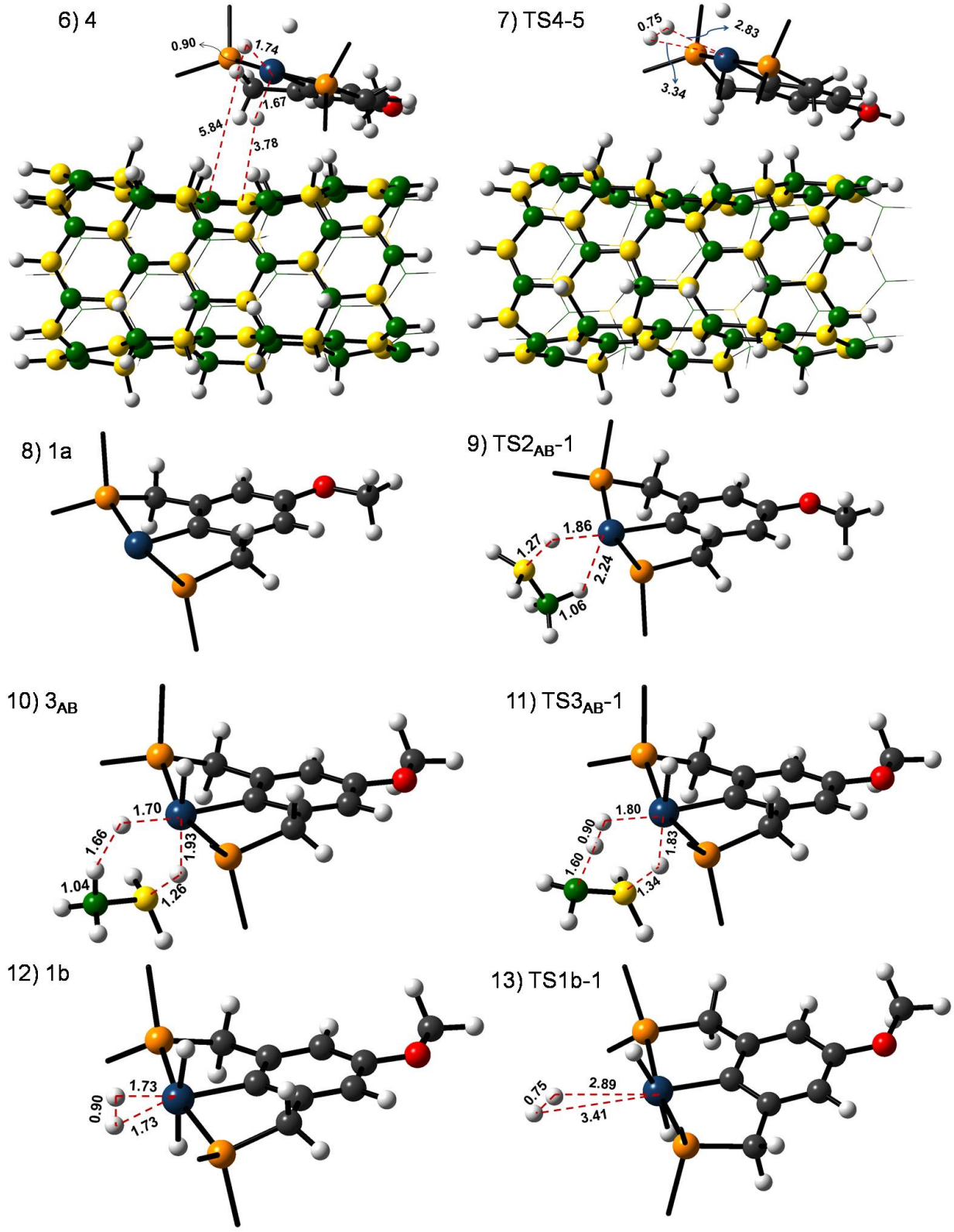
6) 4
0.90
1.74
1.67
5.84
3.78
7) TS4-5
0.75
2.83
3.34
8) 1a
9) TS2$_{AB}$-1
1.27
1.86
2.24
1.06
10) 3$_{AB}$
1.70
1.66
1.93
1.04
1.26
11) TS3$_{AB}$-1
1.80
0.90
1.83
1.60
1.34
12) 1b
1.73
0.90
1.73
13) TS1b-1
0.75
2.89
3.41

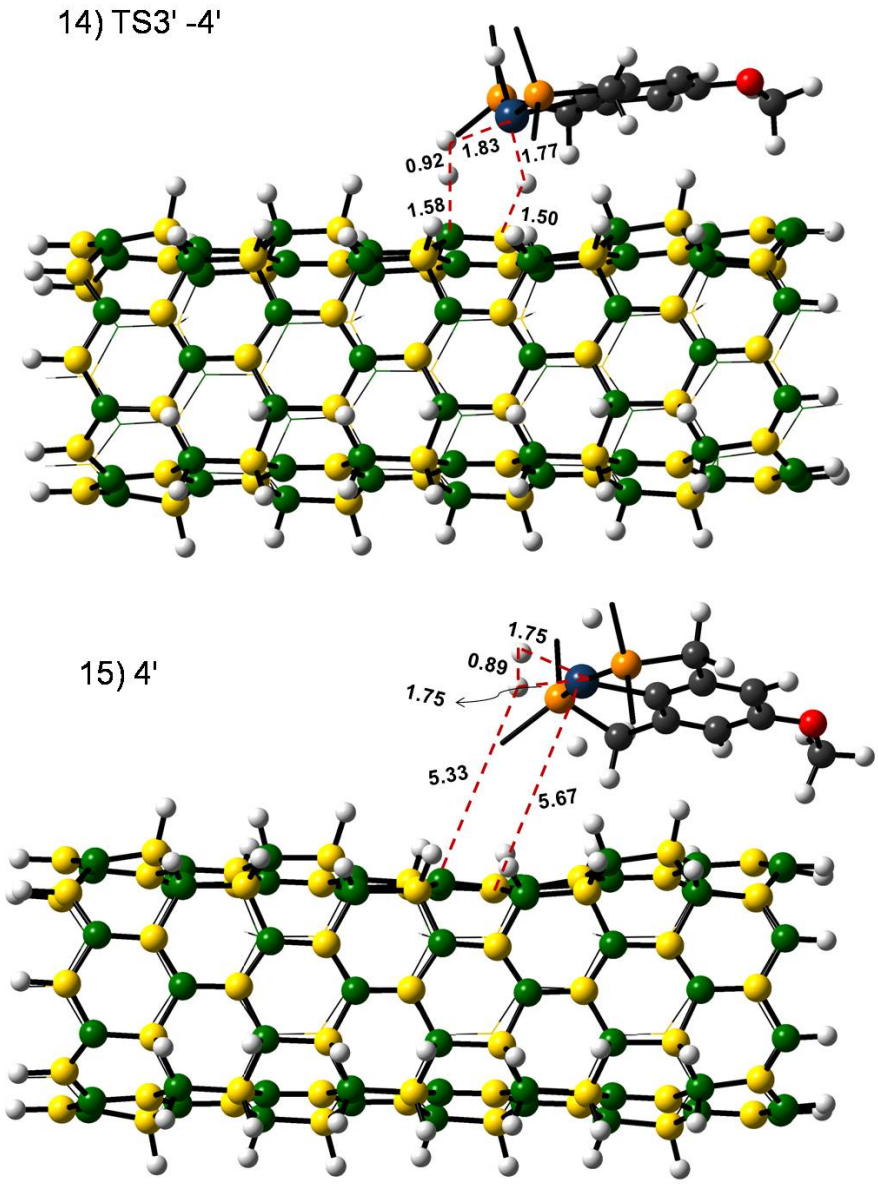

S10) Concerted dehydrogenation: FMO and NBO charge analysis

The dihydride complex **1** and the bare catalyst **1a**, both are bi-functional in nature and can abstract hydride and proton simultaneously. Natural bond orbital charge analysis show that the metal centre is negatively charged in both the catalytic form, while the hydrogen atoms on Ir in **1** are positively charged (see Figure 8). Furthermore, Frontier Molecular Orbital plot displays that the HOMO of intermediate **1** has the largest contribution from Ir d_z^2 and from the s orbital centered on the hydrogen atoms bound to the metal centre. Additionally, the LUMO has substantial contribution from the Ir d_x^2-$_y^2$ orbital. Hence the HOMO-LUMO situation in **1** is conducive for a concerted hydride transfer from B-H on HBNNT to the d_x^2-$_y^2$ orbital on Ir and proton transfer from N-H on HBNNT to the equatorial hydrogen on Ir (see Figure 9).[1, 14] A similar situation arises in **1a** where the HOMO is being delocalized on the $5d_{yz}$ of the transition metal and on the phenyl ring of the OMe-PCP pincer ligand whereas the LUMO has significant Ir d_x^2-$_y^2$ character. The hydride is accepted by the Ir d_x^2-$_y^2$ orbital and the proton goes to the Ir d_{yz} orbital backed by the π – electron density of the aryl carbon.

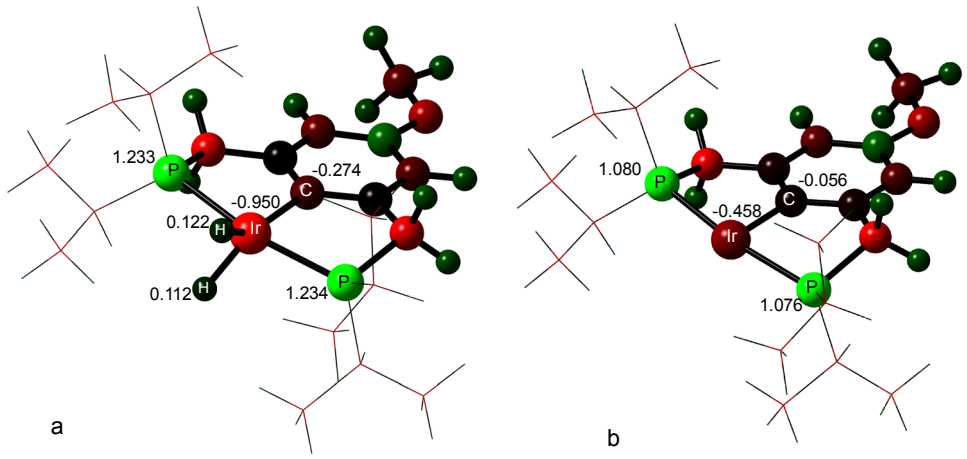

Figure 8. Natural bond orbital charge analysis in a) **1** and b) **1a**. Red to green end of the charge spectrum has been fixed at -1.000 and +1.000 e.s.u charge respectively.

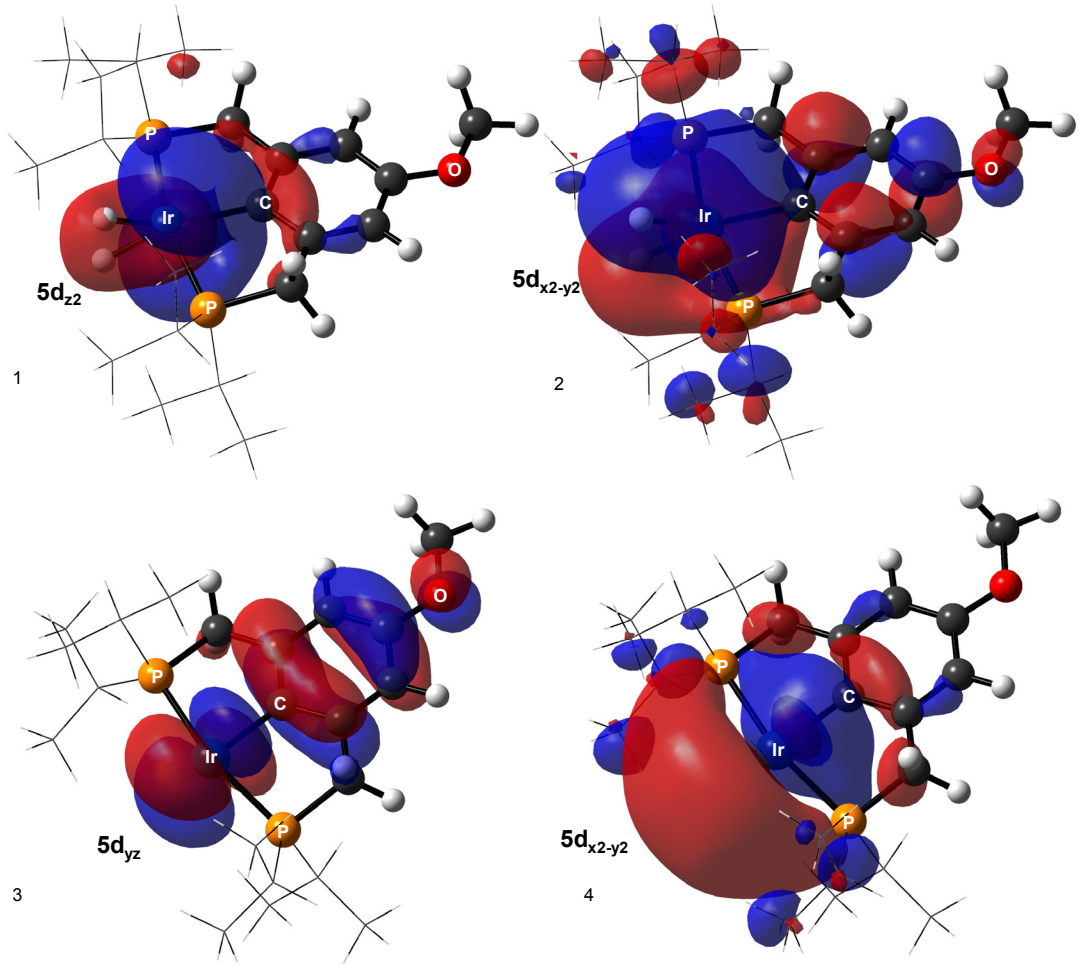

Figure 9. Frontier Kohn-Sham orbital plots: 1)HOMO and 2)LUMO of catalyst **1**. 3)HOMO and 4)LUMO of **1a**. *Iso*propyl groups are shown by wireframe to enhance the visibility of the lobes.

S11) Interaction of the solvent molecule with 1-HBNNT and 1

With a presumption that THF being a polar molecule could be a potential contributor to the alteration of reaction energies (and thereby reaction mechanism), we have looked into probable interaction of the solvent with the chemisorbed hydrogenated BNNT as well as the dihydride catalyst. We found the thermodynamics of the adducts formed between a free THF molecule and 1-HBNNT/**1** is not conducive to trigger an alternate mechanism. THF binds to the Ir centre at a distance of 2.4 Å whereas similar coordination between **1** and a -OMe group takes place at 2.26 Å. This could probably be attributed to the steric encumbrance between the THF moiety and the bulky *iso*propyl groups of the PCP ligands. The binding energy of THF to **1** is -15.6 kcal mol^{-1} (solvent phase zero-point corrected electronic energy) and the free energy change is -9.4 kcal mol^{-1}. We could locate a minimum corresponding to a THF molecule weakly bound to a N-H proton on the surface of a chemisorbed hydrogenated 1-HBNNT. This intermediate lies at $\Delta E(s)_{ZP}$ = -11.2 kcal mol^{-1} and $\Delta G(s)$ = -5.0 kcal mol^{-1} with regard to the initial separated reactants. However in both the cases we find that the adduct formed is less stable than intermediate **3**; $\Delta E(s)_{ZP}$ = -27.8 kcal mol^{-1} and $\Delta G(s)$ = -19.1 kcal mol^{-1} with respect to the initial separated reactants. This clearly suggests that **3** would be the abundant species before dehydrogenation initiates.

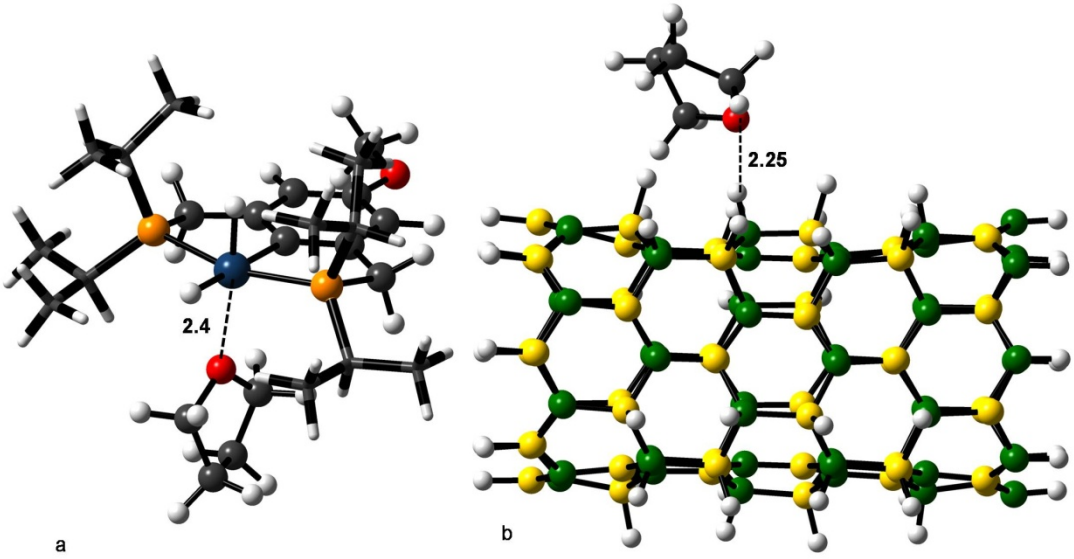

Figure 10. Optimized geometry of the adduct between a) THF and catalyst **1** and b) THF and 1-HBNNT.

S12) Rate determining barriers for desorption of H_2 by Triflic acid

We have conducted optimizations and single point computations of the intermediates and transition states involved in the rate determining step in the desorption of H_2 by Triflic acid from HBNNTs done in our previous study at M06L//B3LYP level of theory.[11b] We found the barriers to be higher than the predicted barriers in this study by 5-6 kcal mol^{-1} and suggests that the design of a proper TM based catalyst would enhance the possibility of concerted removal of hydrogen from HBNNTs and subsequent release of H_2 at a milder condition with faster kinetics. We provide a comparison over here.

RDB ($\Delta G^{\ddagger}$(s)) for 1-HBNNT by Triflic acid and by catalyst **1** at two different levels of theory:

	Triflic acid	Catalyst 1
M06L/B3//B3LYP/B1	20.3	15.6
M06L/B3//B3LYP/B2	19.2	15.6

RDB ($\Delta G^{\ddagger}$(s)) for 2-HBNNT by Triflic acid and by catalyst **1** at two different levels of theory:

	Triflic acid	Catalyst 1
M06L/B3'//B3LYP/B1	23.4	15.7
M06L/B3'//B3LYP/B2'	21.0	15.0

S13) Relaxed Potential Energy Surface Scan for transformation of 4' to 5'

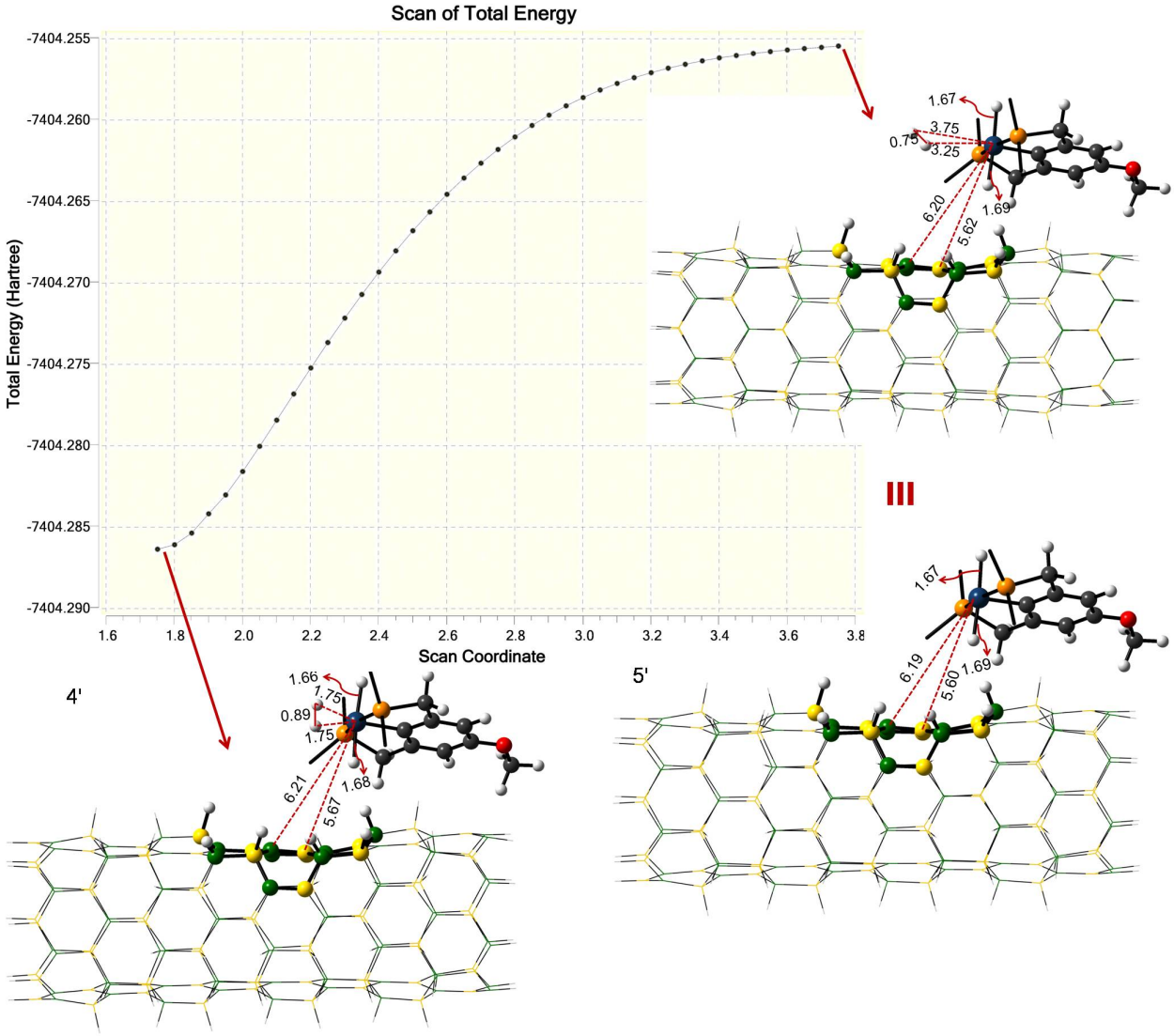

Figure 11. Relaxed Potential Energy Surface Scan for the transformation of **4'** to **5'** showing the relevant geometries.

Attempts to locate a transition state for the transformation of **4'** to **5'** always led to either of the intermediates. Such repeated attempts at various levels of theory strongly suggested us of the absence of any transition state barrier and simple dissociation of H_2 molecule to occur from the tetrahydride Ir species adsorbed on the 2-HBNNT surface. Furthermore, we conducted a relaxed potential energy surface scan, at B3LYP/B1 level of theory (Figure 11), starting from the optimized geometry of **4'** and found no discernible peaks that would indicate a potential transition state structure. We scanned the coordinates to a geometry which has substantially elongated Ir-H_2 distances (being 3.25 and 3.75 Å), much larger than the Ir-H_2 distances in **TS4-5** for 1-HBNNT (which are 2.83 and 3.34 Å). Here we have compared the geometry of **TS4-5** with the last geometry of the linear transit scan leading to **5'** from **4'** because we expect the elongated 2nm long BN nanotube to exhibit similar geometrical parameters as the 1nm long 1-HBNNT. (Please see the optimized geometry of **TS3-4** and **TS3'-4'** in section S9). Moreover, visualization of the last geometry of the scanned structure clearly reveals it to be equivalent to intermediate **5'**. Thus we see that no transition state is present in the pathway leading to the self-dissociation of H_2 dissociation from $Ir(H)_4$ species emanating from intermediate **4'** for the 2-HBNNT case and hence no additional barrier associated with it is predicted. Since the dissociation takes place at $\Delta G(s)$ = 10.3 kcal mol^{-1}, therefore **TS3'-4'** with a free energy barrier of ~ 15 kcal mol^{-1} is predicted to be the rate determining barrier for the dehydrogenation of 2-HBNNT with **1**.

S14) Comparison of the catalyzed to the uncatalyzed dehydrogenation of 1-HBNNT following the associative pathway

Gibbs free energy barriers tabulated are in units of kcal mol^{-1}. For the catalytic pathway, the rate determining barrier (RDB) is chosen.

1st H_2 removal:

	Catalytic (RDB)	Uncatalytic
$\Delta G(g)_{M06L}$	16.9	44.6
$\Delta G(s)_{M06L}$	15.6	41.1
$\Delta G(s)_{M06L\text{-}GD3}$	15.4	40.9
$\Delta G(s)_{B3LYP\text{-}GD3}$	19.4	41.3
$\Delta G(s)_{\omega B97x\text{-}D}$	23.4	42.8

2nd H_2 removal:

	Catalytic (RDB)	Uncatalytic
$\Delta G(g)_{M06L}$	15.1	44.6
$\Delta G(s)_{M06L}$	15.5	40.8
$\Delta G(s)_{M06L\text{-}GD3}$	15.7	40.9
$\Delta G(s)_{B3LYP\text{-}GD3}$	16.4	39.6
$\Delta G(s)_{\omega B97x\text{-}D}$	20.0	42.2

Last H_2 removal:

	Catalytic (RDB)	Uncatalytic
$\Delta G(g)_{M06L}$	14.5	21.1
$\Delta G(s)_{M06L}$	14.0	23.5
$\Delta G(s)_{M06L\text{-}GD3}$	14.0	23.5
$\Delta G(s)_{B3LYP\text{-}GD3}$	14.4	24.6
$\Delta G(s)_{\omega B97x\text{-}D}$	17.2	24.5

We have reported here the rate determining Gibbs free energy barriers for the catalytic removal of H_2 from 1-HBNNT via the associative pathway. We also computed the associated free energy activation barrier with different state-of-the-art hybrid DFT functional incorporating van der Waals interaction. Additionally we have evaluated the free energy barriers for the thermal desorption of hydrogen molecules from the 1-HBNNT surface at the same level of theory. From the tables above we see that the release of hydrogen molecules in a catalytic fashion with subsequent dehydrogenation would occur at barriers generally < 20 kcal mol^{-1} and would therefore be feasible under ambient condition. Alternatively, the uncatalyzed pathway would proceed through predominantly high free energy of activation for both the 1st and 2nd H_2 desorption generally above 40 kcal mol^{-1}. This is probably because the uncatalyzed dehydrogenation occurs through a strained four membered transition state. However, thermally, the last dehydrogenation step would occur at relatively lower barriers (~ 23-24 kcal mol^{-1}). Nevertheless, the catalytic removal of the last H_2 molecule from a mono hydrogenated B-N unit at the middle of a 1nm long BNNT (1-SHBNNT, see Figure 2) would occur at barriers ~ 7-8 kcal mol^{-1} lesser than their uncatalyzed counterpart. The overall energy barriers suggest that the low barrier catalytic pathway by complex **1** would be dominant under moderate conditions.

S15) What would be the barrier for dehydrogenation of hydrogenated BN nanotubes with the *t*Bu pincer catalyst, Ir_{tBu}?

Initially we tried to locate an intermediate analogous to intermediate **3** of a 3c-2e bonded interaction between catalyst $\mathbf{Ir_{tBu}}$ and 1-HBNNT.[11b,12] However, an attempt to investigate such an intermediate failed due to severe steric congestion nearby the metal centre provided by the tertiary butyl groups of the pincer ligand.[11b] The catalytic dihydride Iridium centre drifted apart from the chemisorbed hydrogen of 1-HBNNT. We found that due to the bulky tertiary butyl groups of the phosphine moiety, the metal centre cannot come in close proximity to the B-H and N-H hydrogen on the surface of 1-HBNNT. We provide comparison of the structures obtained with 1-HBNNT and AB with $\mathbf{Ir_{tBu}}$ and complex **1** in Figure 12. Since no initial binding of the catalyst is predicted to occur with density functional calculations, we therefore hypothesize that the barrier for H_2 release with *t*Bu pincer catalyst would essentially be those predicted for thermal uncatalyzed desorption of H_2 from HBNNTs (see section S14). Thus the barriers with $\mathbf{Ir_{tBu}}$ would be high, and much larger than the predicted barrier for *i*Pr pincer complex (**1**) catalyzed pathway. We propose that the less bulky complex **1** would be more efficient in releasing chemisorbed hydrogen from hydrogenated BN nanotube at moderate conditions.

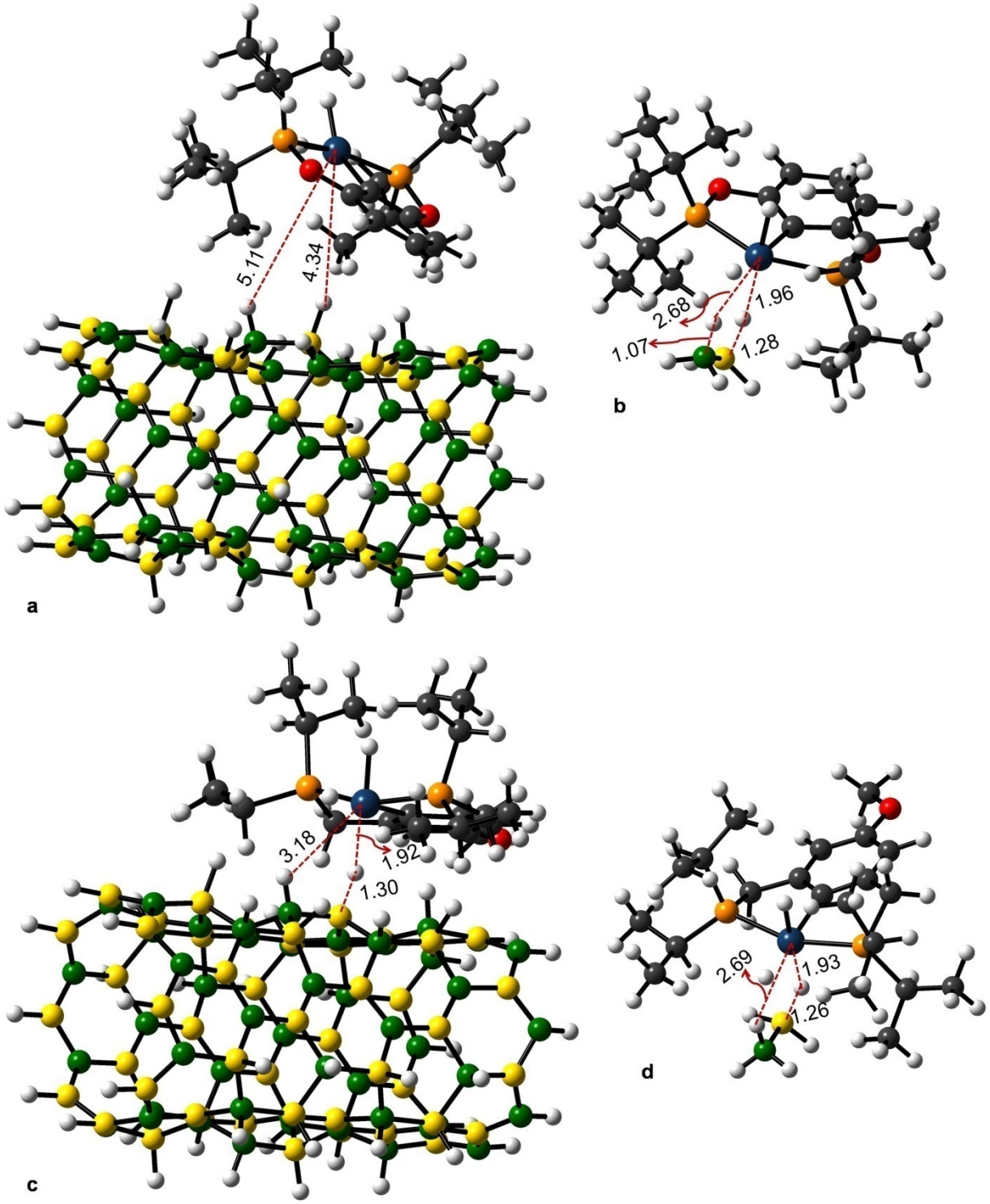

Figure 12. Optimized geometry of the initial intermediate found with a) 1-HBNNT and $\mathbf{Ir}_{\mathbf{tBu}}$, b) AB and $\mathbf{Ir}_{\mathbf{tBu}}$, c) 1-HBNNT and catalyst **1** and d) AB and catalyst **1**.

S16) Steric factor decides reaction of HBNNTs with potential amine borane dehydrogenating catalysts

We also intended to explore the reactivity of other conventional transition metal based catalysts towards hydrogenated BN nanotubes which are apt at dehydrogenation of amine boranes in general. Among them, a well known Ru-based catalyst designed by Fagnou *et al.*[15] was found to dehydrogenate AB via treatment of KO^{t}Bu in THF medium. However, instead of taking the actual catalysts (with bulky substituents as represented by Figure 13a), for computational purpose, the authors have employed catalyst prototype given in Figure 13b, with a presumption that outer-sphere hydrogen transfer would lead to an amide ligand formation on the Ru metal. We tried to investigate a similar reaction pathway as depicted in the mentioned article with the actual *i*Pr$_2$P ligated Ruthenium catalyst as shown in Figure 13a.

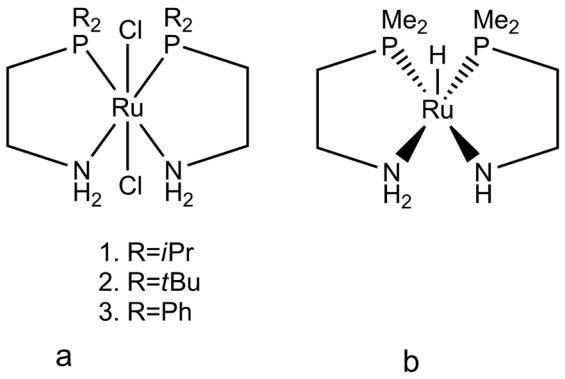

Figure 13. Representation of the a) actual catalysts and b) catalyst prototype designed by Fagnou *et al.* for dehydrogenation of AB.

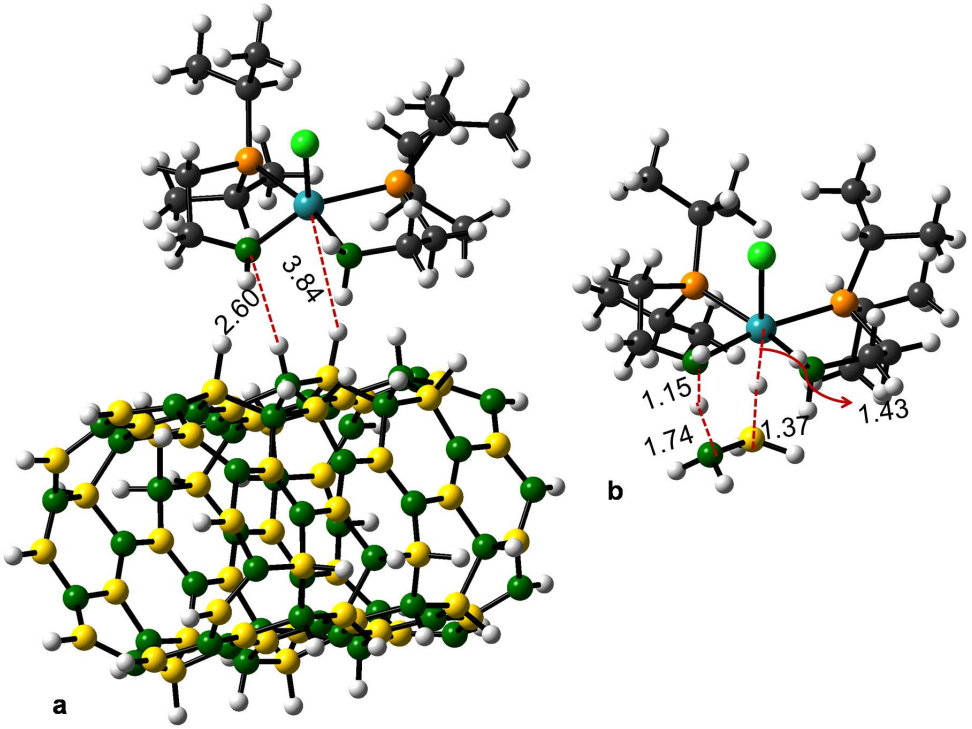

Figure 14. Optimized geometry of the initial intermediate found with the Ruthenium based catalyst designed by Fagnou *et al.* with a) 1-HBNNT and b) AB.

Akin to the fate observed for the minimum of $\mathbf{Ir_{tBu}}$ with 1-HBNNT we find that an attempt to locate an intermediate of initial interaction of the Ru-catalyst resulted in a larger separation of the catalyst from the reactivity centre. Our computational investigation revealed that the geometrical parameters are very different for those found with AB and with 1-HBNNT (Figure 14). As favourable binding to the B-H and N-H bond to the catalyst is not observed it is obvious that steric effects would also prohibit low barrier catalytic release of H_2.

We initiated a similar minimum search with the Fe pincer complex designed by Hairong Guan and group[16] where the authors have proposed a mechanistic pathway involving release of a bulky phosphine (PMe_2Ph) moiety from one of the axial positions of the octahedral metal complex, before coordination to ammonia borane (see Figure 15). In this case also, we found that the catalyst could not be accommodated well on the surface of the BN nanotube due to the existing bulky PMe_2Ph on the equatorial position of the metal centre which provides a steric impediment with the hydrogen on the exterior surface of the nanotube (Figure 16). For comparison we have also provided the optimized geometry of the intermediate found with the aforementioned catalyst binding to ammonia borane.

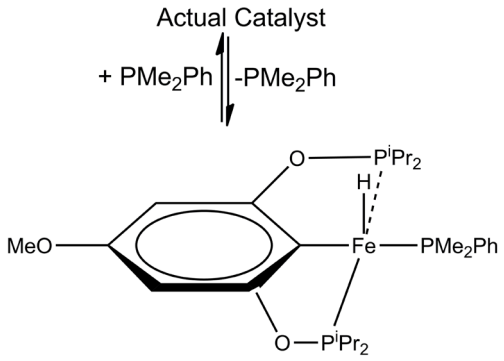

Figure 15. Representation of the Fe pincer catalyst of Guang et al.

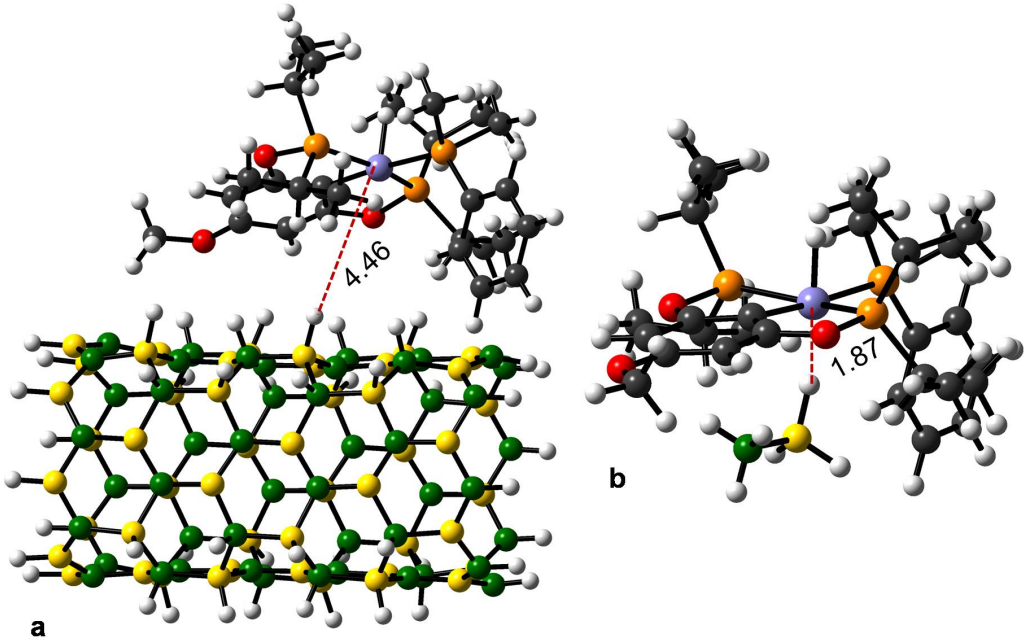

Figure 16. Optimized geometry of the initial intermediate found with the Fe pincer catalyst designed by Guang *et al.* with a) 1-HBNNT and b) AB.

Other efficient amine borane dehydrogenating agents include Kim's Palladium catalyst,[17] Ruthenium catalyst[18] designed by Travis J. Williams and the Molybdenum catalyst[19] designed by Agapie. The mechanistic working of the Pd catalyst is not well understood. Even repeated attempts by us have failed to produce some proper directions regarding the ammonia-borane dehydrogenation mechanism by Kim's Palladium catalyst. Moreover, the authors indicate that the spent fuel of ammonia borane dehydrogenation consists of B-B bonded species whose formation would not be possible for dehydrogenated BNNTs. Hence, it was reasonable not to choose this catalyst for nanotube dehydrogenation. Furthermore, we found the Ruthenium catalyst and the Molybdenum catalyst also drifted away from the BN nanotube.

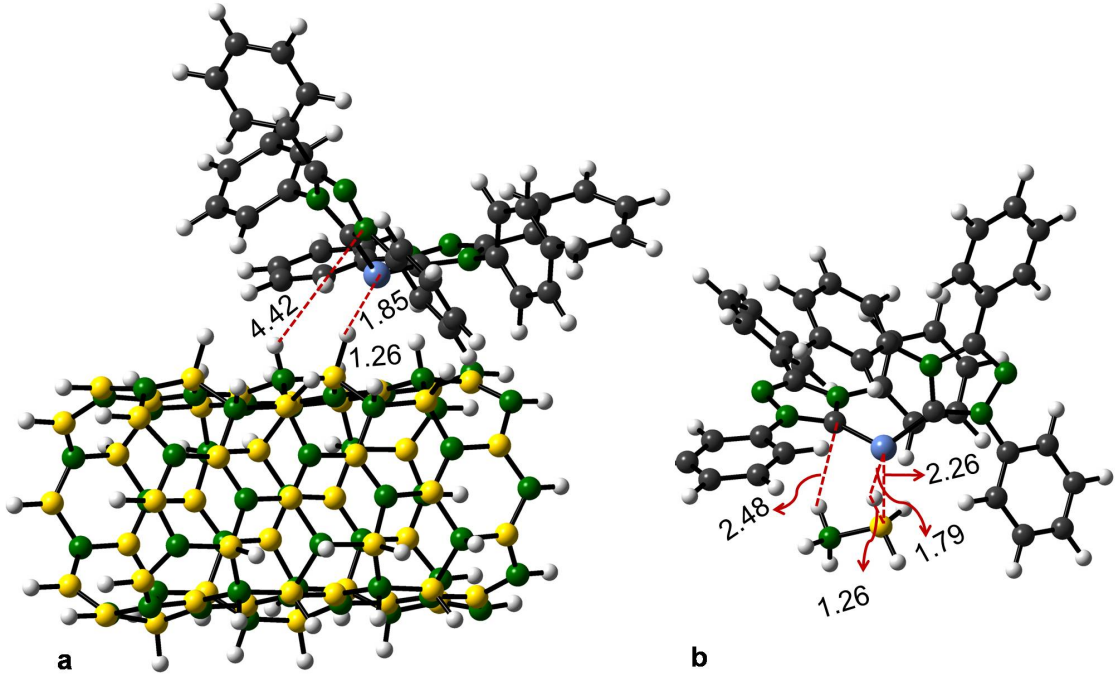

Figure 17. a) Optimized geometry of the initial intermediate found with the $Ni(NHC)_2$ catalyst designed by Baker *et al.* with a) 1-HBNNT and b) Predicted structure of the initial binding of $Ni(NHC)_2$ catalyst with AB as reported by Yang and Hall .[21b]

We embarked on investigating plausible initial interaction of another well-known dehydrogenating catalyst, the $Ni(NHC)_2$ system.[20] However, the mechanism of AB dehydrogenation by this catalyst is debatable since there are contradictory proposed pathways by Zimmerman *et al.*[21a] and Hall *et al.*[21b], both undertaking low-barrier conduits. Furthermore has proposed a different mechanism for ammonia-borane dehydrogenation in the $Ni(NHC)_2$ catalyst which involves a free NHC released in the medium by the action of ammonia-borane on the $Ni(NHC)_2$ catalyst.[21c] In order to fully understand the mechanism of dehydrogenation of amine boranes by this nickel catalyst, extensive experimental efforts would also be required. Nonetheless, following a mechanistic pathway as shown by Hall *et al.*[21b] we attempted to figure out a stable intermediate of $Ni(NHC)_2$ with 1-HBNNT as has been predicted for AB where the metal centre coordinates to the B-H bonds in a σ-complex. In the following step Yang and Hall predicts the proton from the N end to move to one of the carbene carbon.[21b] However to our dismay, we find that optimizations of the nanotube with the $Ni(NHC)_2$ catalyst does not render a favorable interaction between the carbene carbon and the N-H bond. Also no Ni-B bond is exhibited in the optimized structure of the catalyst with the nanotube as has been predicted for AB. We have presented a comparison of the geometries of AB and 1-HBNNT with the $Ni(NHC)_2$ in Figure 17 which involve very different bond parameters. This probably suggests that mechanism proposed by Hall *et al.* is not likely to operate.[17b]

Also the feeble interaction between the HBNNT and $Ni(NHC)_2$ suggests that the formation of a free NHC analogous to the mechanism predicted by Zimmerman *et al.* would not be possible in this case. The strategy of nanotube dehydrogenation by $Ni(NHC)_2$ is a different chemical problem and would be dealt separately in a future work and is certainly beyond the scope of this communication.

Density functional studies on the initial binding of all these catalysts with hydrogenated BN nanotube suggests that bulky groups adjacent to the metal centre hovering over the chemisorbed hydrogen would prohibit strong adduct formation. We find all these catalysts (except the Goldman catalyst[2] represented by **1** in the main text) did not show any strong Metal-Hydride-Boron bonding, rather preferred to get distant from the hydrides and protons of the adjacent B-N bonds. Due to steric encumbrance, catalysts which are well-known for Ammonia Borane dehydrogenation would be physically unsuitable to bind to the chemisorbed hydrogen of HBNNTs and catalyze the removal of these hydrogen atoms. However computational catalyst design can be used to overcome this hurdle. We feel that the Fe-pincer catalyst which has equivalent structural framework as the iridium pincer complex would be cheaper alternative for nanotube dehydrogenation had there been less bulky phosphine moieties attached to the metal centre on the equatorial position. But synthesis and design of such preferred catalyst would require extensive efforts from the experimental community and the current literature is devoid of suitable Fe pincer catalyst with less bulky ligands.

From our extensive computations, it is hypothesized that not all the TM based catalysts found in the literature for AB dehydrogenation would give low barrier conduits for H_2 release from hydrogenated BN nanotube. For suitable binding of the catalyst to the hydrides and protons over nanotube, the steric effects should be overcome. Moreover, less steric hindrance also does not always guarantee low energy of activation. Such property depends on the efficiency of the catalyst and its ability to work under ambient conditions.

S17) Gaussian 09 full citation

[1] Gaussian 09, Revision A.02, M. J. Frisch, G. W. Trucks, H. B. Schlegel, G. E. Scuseria, M. A. Robb, J. R. Cheeseman, G. Scalmani, V. Barone, B. Mennucci, G. A. Petersson, H. Nakatsuji, M. Caricato, X. Li, H. P. Hratchian, A. F. Izmaylov, J. Bloino, G. Zheng, J. L. Sonnenberg, M. Hada, M. Ehara, K. Toyota, R. Fukuda, J. Hasegawa, M. Ishida, T. Nakajima, Y. Honda, O. Kitao, H. Nakai, T. Vreven, J. A. Montgomery, Jr., J. E. Peralta, F. Ogliaro, M. Bearpark, J. J. Heyd, E. Brothers, K. N. Kudin, V. N. Staroverov, R. Kobayashi, J. Normand, K. Raghavachari, A. Rendell, J. C. Burant, S. S. Iyengar, J. Tomasi, M. Cossi, N. Rega, J. M. Millam, M. Klene, J. E. Knox, J. B. Cross, V. Bakken, C. Adamo, J. Jaramillo, R. Gomperts, R. E. Stratmann, O. Yazyev, A. J. Austin, R. Cammi, C. Pomelli, J. W. Ochterski, R. L. Martin, K. Morokuma, V. G. Zakrzewski, G. A. Voth, P. Salvador, J. J. Dannenberg, S. Dapprich, A. D. Daniels, O. Farkas, J. B. Foresman, J. V. Ortiz, J. Cioslowski, and D. J. Fox, Gaussian, Inc., Wallingford CT, 2009.

[2] Gaussian 09, Revision D.01, M. J. Frisch, G. W. Trucks, H. B. Schlegel, G. E. Scuseria, M. A. Robb, J. R. Cheeseman, G. Scalmani, V. Barone, B. Mennucci, G. A. Petersson, H. Nakatsuji, M. Caricato, X. Li, H. P. Hratchian, A. F. Izmaylov, J. Bloino, G. Zheng, J. L. Sonnenberg, M. Hada, M. Ehara, K. Toyota, R. Fukuda, J. Hasegawa, M. Ishida, T. Nakajima, Y. Honda, O. Kitao, H. Nakai, T. Vreven, J. A. Montgomery, Jr., J. E. Peralta, F. Ogliaro, M. Bearpark, J. J. Heyd, E. Brothers, K. N. Kudin, V. N. Staroverov, T. Keith, R. Kobayashi, J. Normand, K. Raghavachari, A. Rendell, J. C. Burant, S. S. Iyengar, J. Tomasi, M. Cossi, N. Rega, J. M. Millam, M. Klene, J. E. Knox, J. B. Cross, V. Bakken, C. Adamo, J. Jaramillo, R. Gomperts, R. E. Stratmann, O. Yazyev, A. J. Austin, R. Cammi, C. Pomelli, J. W. Ochterski, R. L. Martin, K. Morokuma, V. G. Zakrzewski, G. A. Voth, P. Salvador, J. J. Dannenberg, S. Dapprich, A. D. Daniels, O. Farkas, J. B. Foresman, J. V. Ortiz, J. Cioslowski, and D. J. Fox, Gaussian, Inc., Wallingford CT, 2013.

S18) References

[1] A. Paul, C. B. Musgrave, *Angew. Chem. Int. Ed.,* 2007, **46**, 8153.
[2] a) K. Zhu, P. D. Achord, X. Zhang, K. Krogh-Jespersen, A. S. Goldman, *J. Am. Chem. Soc.,* 2004, **126**, 13044; b) K. Krogh-Jespersen, M. Czerw, N. Summa, K. B. Renkema, P. D. Achord, A. S. Goldman, *J. Am. Chem. Soc.,* 2002, **124**, 11404.
[3] K. Ghatak, M. Mane, K. Vanka, *ACS Catal*., 2013, **3**, 920.
[4] a) G. Mpourmpakis, E. Tylianakis, G. E. Froudakis, *Nano Lett.,* 2007, **7**, 1893; b) G. Mpourmpakis, G. E. Froudakis, *Catal. Today,* 2007, **120**, 341; c) Md T. Baei, A. R. Soltani, A. V. Moradi, E. T. Lemeski, *Comp. Theo. Chem.,*. 2011, **970**, 30.
[5] a) Z. Chen, S. Nagase, A. Hirsch, R. C Haddon, W. Thiel, P. v. R. Schleyer, *Angew. Chem.* 2004, **116**, 1578; b) J. Bai, X. C. Zeng, H. Tanaka, J. Y. Zeng, *Proc. Nat. Ac. Sci.,* 2004, **101**, 2664.
[6] K. Fukui, *Acc. Chem. Res.,* 1981, **14**, 363.
[7] a) A. D. Becke, *J. Chem. Phys.,* 1993, **98**, 5648; b) Y. Zhao, D. G. Truhlar, *J. Chem. Phys.,* 2006, **125**, 194101; c) D3 version of Grimme's dispersion with the original D3 damping function included with the parameter EmpiricalDispersion=GD3 along with the M06L or B3LYP keyword in Gaussian 09, Revision D.01; S. Grimme, *J. Comp. Chem.,* 2006, **27**, 1787; d) J.-D. Chai, M. Head-Gordon, *Phys. Chem. Chem Phys.,* 2008, **10**, 6615.
[8] a) V. Barone, M. Cossi, *J. Phys. Chem. A,* 1998, **102**, 1995; b) M. Cossi, N. Rega, G. Scalmani, V. Barone, *J. Comp. Chem.*, 2003, **24**, 669.
[9] M. C. Denney, V. Pons, T. J. Hebden, D. M. Heinekey, K. I. Goldberg, *J. Am. Chem. Soc.,* 2006, **128**, 12048.
[10] a) R. L. Martin, P. J. Hay, L. R. Pratt, *J. Phys. Chem. A,* 1998, **102**, 3565; b) D. H. Wertz, *J. Am. Chem. Soc.,* 1980, **102**, 5316; c) C. Spickermann, "Entropies of Condensed Phases and Complex Systems", *Springer Theses*, 2010, **Chapter 3**, 76 and references therein. d) Z.-X. Yu, K. N. Houk, *J. Am. Chem. Soc.,* 2003, **125**, 13825.
[11] a) L. Roy, S. Mittal, A. Paul, *Angew. Chem. Int. Ed.,* 2012, **51**, 4152; b) L. Roy, S. Bhunya, A. Paul, *Angew. Chem. Int. Ed.,* 2014, **53**, 12430; c) H. Li, X. Wang, F. Huang, G. Lu, J. Jiang, Z.-X. Wang, *Organometallics,* 2011, **30**, 5233.
[12] I. Gottker-Schnetmann, P. White, M. Brookhart, *J. Am. Chem. Soc.,* 2004, **126**, 1804.
[13] D. Morales-Morales, C. Grause, K. Kasaoka, R. Redón, R. E. Cramer, C. M. Jensen, *Inorg. Chim. Acta*, 2000, **300–302**, 958.
[14] S. Bhunya, T. Malakar, A. Paul, *Chem. Commun.,* 2014, **50**, 5919.
[15] N. Blaquiere, S. Diallo-Garcia, S. I. Gorelsky, D. A. Black, K. Fagnou, *J. Am. Chem. Soc*., 2008, **130**, 14034.
[16] P. Bhattacharya, J. A. Krause, H. Guan, *J. Am. Chem. Soc.* 2014, **136**, 11153.
[17] S.-K. Kim, W.-S. Han, T.-J. Kim, T.-Y. Kim, S. W. Nam, M. Mitoraj, L. Piekoś, A. Michalak, S.-J. Hwang, S. O. Kang, *J. Am. Chem. Soc.*, 2010, **132**, 9954.
[18] B. L. Conley, D. Guess, T. J. Williams, *J. Am. Chem. Soc.*, 2011, **133**, 14212.
[19] J. A. Buss, G. A. Edouard, C. Cheng, J. Shi, T. Agapie, *J. Am. Chem. Soc.* 2014, **136**, 11272.
[20] R. J. Keaton, J. M. Blacquiere, R. T. Baker, J. Am. Chem. Soc., 2007, **129**, 1844.
[21] a) P. M. Zimmerman, A. Paul, C. B. Musgrave, *Inorg.Chem*., 2009, **48**, 5418; b) X. Yang, M. B. Hall, *J. Am. Chem. Soc.,* 2008, **130**, 1798; c) P. M. Zimmerman, A. Paul, Z. Zhang, C. B. Musgrave, *Angew. Chem. Int. Ed.,* 2009, **48**, 2201.